Penetrable Square-Well fluids: Exact results in one dimension

Andrés Santos*

Departamento de Física, Universidad de Extremadura, E-06071 Badajoz, Spain

Riccardo Fantoni† and Achille Giacometti‡

Dipartimento di Chimica Fisica, Università di Venezia,
Calle Larga S. Marta DD2137, I-30123 Venezia, Italy

(Dated: April 23, 2008)

We introduce a model of attractive penetrable spheres by adding a short range attractive square well outside a penetrable core, and we provide a detailed analysis of structural and thermodynamical properties in one dimension using the exact impenetrable counterpart as a starting point. The model is expected to describe star polymers in regimes of good and moderate solvent under dilute conditions. We derive the exact coefficients of a low density expansion up to second order for the radial distribution function and up to fourth order in the virial expansion. These exact results are used as a benchmark to test the reliability of approximate theories (Percus-Yevick and hypernetted chain). Notwithstanding the lack of an exact solution for arbitrary densities, our results are expected to be rather precise within a wide range of temperatures and densities. A detailed analysis of some limiting cases is carried out. In particular we provide a complete solution of the sticky penetrable-sphere model in one dimension up to the same order in density. The issue of Ruelle's thermodynamics stability is analyzed and the region of a well defined thermodynamic limit is identified.

I.   INTRODUCTION

Unlike simple liquids, where two-body potentials describe interactions at the atomistic levels, complex liquid interactions are always a result of an average process over the microscopic degrees of freedom. As a result, highly simplified models often accurately describe a number of experimental features ranging from structural to thermophysical properties. Examples include colloidal dispersions, macromolecules, and combinations of the two [1]. A noteworthy feature of these system is that the hard-core repulsive barrier for very short range is not an essential ingredient of the model. In the case of highly ramified polymers in good solvent (star polymers), for instance, the center-of-mass of two polymer chains can be at a distance much smaller than their respective radii of gyration and they are well described by an effective Gaussian interaction [2]. The simplest of this class of minimal bounded potential is the so-called penetrable spheres (PS) [3] that has attracted considerable attention in the last few years (see e.g. Ref. [4] and references therein). In this case the infinite barrier of the hard sphere (HS) potential is replaced by a finite one, thus allowing for a finite probability of penetrating inside the core.

A major advantage of the PS potential is, of course, simplicity. On the other hand, it lacks an attractive part which is expected to be relevant in such a complex environment in view of the ubiquity of van der Waals dispersion forces. The purpose of the present work is to address this point by proposing a variation of the PS model in which a square well (SW) is added outside the core. This model, hereafter referred to as penetrable square-well (PSW), has an extremely rich phenomenology notwithstanding its simplicity, including a number of interesting limiting cases as will be discussed later on.

One-dimensional bounded interactions do not belong to the class of nearest-neighbor fluids for which the total potential energy can be written as

$$U_N(x_1, \ldots, x_N) = \sum_{i=1}^{N-1} \phi(|x_{i+1} - x_i|) , \tag{1.1}$$

where $\phi(r)$ is the pair potential and $\{x_i, i = 1, \ldots, N\}$ are the coordinates of the N particles confined in a segment of length L, which eventually may be let to go to infinity. A necessary (but not sufficient) condition for a one-dimensional

fluid to satisfy Eq. (1.1) is to be a hard-core fluid, i.e., a fluid made of particles which cannot penetrate one another due to the existence of an infinite repulsive potential barrier in $\phi(r)$.

Nearest-neighbor fluids admit an analytic exact statistical-mechanical solution in one-dimension [5]: the partition function, equation of state, and correlation functions of any order can be calculated analytically from the knowledge of the pair potential. In addition to HS [5, 6, 7, 8, 9, 10], both structural and thermophysical properties can be analytically obtained in one dimension for Baxter's sticky hard-sphere (SHS) potential [11, 12], and for the SW potential [13], but the technique permits in principle the analysis of a large class of nearest-neighbor one-dimensional potentials.

In the absence of the nearest-neighborhood constraint (as happens with bounded potentials), the situation is far more complex and we are not aware of any general analytical approach to the problem, even in one dimension. As a matter of fact there exist only a few examples of analytically solvable one-dimensional models of this type, which include the Kac potential [14] and the Coulomb potential [15, 16]. For PS, it was observed [4, 17] that the exact analytic solution for HS can be efficiently exploited to build a rather precise, albeit approximate, solution of the penetrable counterpart. This analysis is here extended to PSW interactions. Using a low density expansion and the corresponding exact solution for the SW problem, we derive the exact result up to the second order in a density expansion of the radial distribution function and up to fourth order in the virial expansion of the equation of state. These exact low density calculations are contrasted with approximate theories such as the Percus-Yevick (PY) and the hypernetted chain (HNC) closures, thus providing an assessment on the relative reliability of both approximations and the low density expansion. As a preliminary simplified step to our calculation, we also examine the penetrable counterpart of the SHS problem, denoted as sticky penetrable spheres (SPS) in the following, which provides a guideline to tackle the more difficult PSW problem.

The introduction of an attractive part of the potential into a penetrable interaction raises the important issue of the existence of a well defined thermodynamic limit [18, 19]. We address this problem for the PSW model and provide compelling arguments to identify the stability region, which is guaranteed for a sufficiently small (≈ 0.5) ratio between the attractive and repulsive energy scales and arbitrary values of the other parameters.

The remaining of the paper is structured as follows. In Section II we introduce the model along with all its limiting cases (including the SPS fluid) and we study its stability. Section III briefly accounts for the main equations necessary for the analytical solution of the nearest-neighbor class of fluids with arbitrary interactions. The exact solution of the one-dimensional SHS potential is derived within this general approach in Section III B and this is used to obtain the corresponding low density solution of the SPS in Section IV. A similar analysis is carried out in Section V for PSW and the results are contrasted with those stemming from PY and HNC closures. Section VII contains some closing remarks, whereas some of the more technical details are confined in suitable appendices.

II. THE PENETRABLE SQUARE-WELL (PSW) MODEL

The penetrable square-well (PSW) model is defined by the following pair potential (see Fig. 1)

$$\phi\left(r\right) = \begin{cases} +\epsilon_r, & r < \sigma, \\ -\epsilon_a, & \sigma < r < \sigma + \Delta, \\ 0, & r > \sigma + \Delta, \end{cases} \tag{2.1}$$

where ϵ_r and ϵ_a are two positive constants accounting for the repulsive and attractive parts of the potential, respectively. Here σ is the diameter of the sphere (length of the rod in one dimension) and $\Delta < \sigma$ is the width of the well. This model has a number of relevant limiting cases. When $\epsilon_r \to \infty$ it reduces to a square-well (SW) fluid, whereas $\epsilon_a \to 0$ yields the penetrable-sphere (PS) model studied in Ref. [4] in the one-dimensional case. In addition it gives rise to an interesting variation, referred to as "sticky penetrable spheres" (SPS), within an appropriate limit of infinite well depth of vanishing width (see below). Finally, we recover the hard-sphere (HS) fluid in the combined limit $\epsilon_r \to \infty$ and $\epsilon_a \to 0$.

It is worthwhile noting that the PSW model (and its variants) considered here is different from other apparently similar models like the Widom-Rowlinson's of interpenetrating spheres [20], the concentric-shell model [21], or the permeable-sphere model [22],

As usual, a very important role is played by the Mayer function

$$f\left(r\right) = e^{-\beta\phi(r)} - 1, \tag{2.2}$$

where $\beta = 1/k_B T$ is the inverse of the thermal energy (k_B is the Boltzmann constant and T is the absolute tempera-
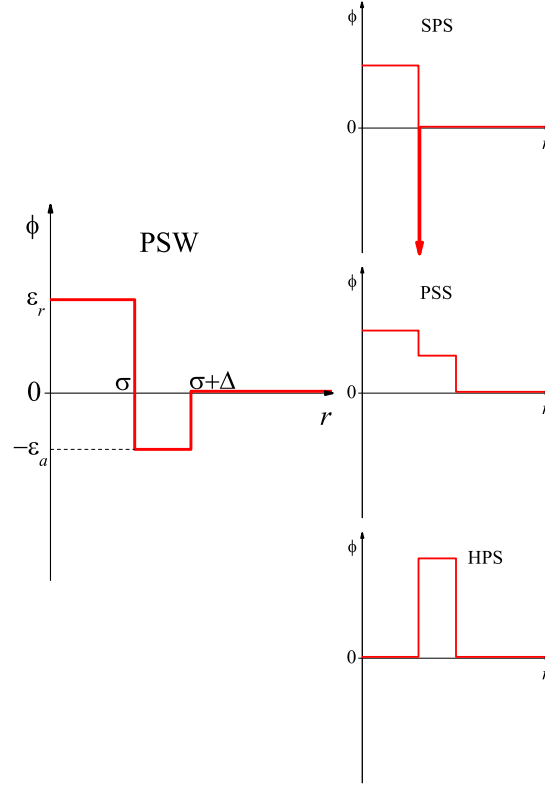
FIG. 1: (Color online) Sketch of the penetrable square-well (PSW) potential (left column). The right column shows a few limiting cases: the sticky penetrable spheres (SPS) potential ($\epsilon_a \to \infty$ and $\Delta \to 0$), the penetrable square-shoulder (PSS) potential ($\epsilon_r > -\epsilon_a > 0$), and the hollow hard-spheres (HPS) potential ($\epsilon_r = 0$ and $\epsilon_a < 0$).

ture). In the present model, this becomes

$$
\begin{aligned}
f(r) &= \begin{cases} -\gamma_r, & r < \sigma, \\ +\gamma_a, & \sigma < r < \sigma + \Delta, \\ 0, & r > \sigma + \Delta, \end{cases} \\
&= \gamma_r f_{\mathrm{HS}}(r) + \gamma_a[\Theta(r-\sigma) - \Theta(r-\sigma-\Delta)] ,
\end{aligned}
\tag{2.3}
$$

where

$$
\gamma_r = 1 - e^{-\beta \epsilon_r}
\tag{2.4}
$$

is the parameter measuring the degree of penetrability varying between 0 (free penetrability) and 1 (impenetrability) and

$$
\gamma_a = e^{\beta \epsilon_a} - 1
\tag{2.5}
$$

plays a similar role for the attractive part. Here $f_{\mathrm{HS}}(r) = \Theta(r-\sigma) - 1$ is the Mayer function for a HS model, which can then be recovered in the limit $\gamma_r \to 1$ and $\gamma_a \to 0$, and $\Theta(r)$ is the usual step function equal to 1 for $r > 0$ and 0 otherwise. It also proves convenient to introduce the ratio $\gamma = \gamma_a/\gamma_r$ which is a measure of the depth of the attractive well, relative to the "penetrability" of the core. In that way, Eq. (2.3) can be rewritten as

$$
\begin{aligned}
f(r) &= \gamma_r \left\{ f_{\mathrm{HS}}(r) + \gamma[\Theta(r-\sigma) - \Theta(r-\sigma-\Delta)] \right\} \\
&= \gamma_r f_{\mathrm{SW}}(r),
\end{aligned}
\tag{2.6}
$$

where $f_{\mathrm{SW}}(r)$ is the Mayer function of a SW fluid with the change $\gamma_a \to \gamma$.

Although the PSW model can be defined for any dimensionality of the system, throughout the remainder of this paper we will specialize to the one-dimensional case.

TABLE I: Summary of the models.

Model	Acronym	ϵ_r	ϵ_a	Δ
Penetrable Spheres	PS	> 0	0	> 0
Penetrable Square-Well	PSW	> 0	> 0	> 0
Sticky Penetrable Spheres	SPS	> 0	$\to +\infty$	$\to 0$
Penetrable Square-Shoulder	PSS	> 0	< 0	> 0
Hollow Penetrable Spheres	HPS	0	< 0	> 0
Hollow Hard Spheres	HHS	0	$\to -\infty$	> 0

A. The thermodynamic stability issue

As anticipated in the Introduction, in our model we need to make sure that the system is always *stable* in the sense that the total energy is always bounded from below by $-NB$, N being the number of particles and B being an arbitrary positive constant [19]. The physical origin of such an instability can be traced back to the fact that a soft core allows the possibility of a "collapsed-state" where the energy is no longer proportional to the number of particles N and a well-defined thermodynamic limit may not exist. In a classic paper, Fisher and Ruelle [18] provided a set of conditions on the pair potentials which are sufficient for stability, but the actual implementation of such conditions in soft-core systems is far from being trivial as was recently shown for Gaussian-core models [23] and Lennard-Jones fluids [24].

In the PSW model, the issue is clearly related to the interplay between the two energy scales, ϵ_r and ϵ_a, for the repulsive and attractive parts of the potential. As shown in Appendix A, we predict that the system *might be unstable* when $\epsilon_r < 2\epsilon_a$ whereas we prove that it is *certainly stable* in the opposite case $\epsilon_r > 2\epsilon_a$.

B. The sticky limit: the SPS model

It is instructive at this point to consider a particular limit of the PSW model which will be referred to as the sticky penetrable-sphere (SPS) model (see Fig. 1). This is a variation of a widely used *sticky hard-sphere* (SHS) model introduced long time ago by Baxter [25], which has proven to be extremely useful in the framework of complex fluids, recently even in its anisotropic version [26]. The simplest way of introducing it is at the level of the Mayer function [see Eq. (2.3)], which becomes

$$f_{\text{SHS}}\left(r\right) \;=\; f_{\text{HS}}\left(r\right) + \alpha\sigma\delta_+\left(r - \sigma\right) \tag{2.7}$$

where

$$\delta_+\left(r\right) \;=\; \lim_{a\to 0^+}\frac{\Theta(r) - \Theta(r - a)}{a}, \tag{2.8}$$

The relation with the SPS model is then provided by

$$f_{\text{SPS}}\left(r\right) \;=\; \gamma_r f_{\text{SHS}}\left(r\right) \tag{2.9}$$

In the original SHS model [25], $\alpha = 1/12\tau > 0$, (τ playing the role of an effective temperature) but the connection with the PSW model is readily achieved from Eq. (2.6) by considering the limits $\Delta \to 0$ and $\epsilon_r \to \infty$ so that $\alpha = (\gamma_a/\gamma_r)(\Delta/\sigma)$ remains finite. In spite of its usefulness, the SHS model is known to suffer from some mathematical drawbacks, the most important of them being that it is unstable in spatial dimensions greater than 1, as pointed out by Stell [27], in view of the divergence of the virial coefficient corresponding to a close packed configuration. For the SPS model we will be able to achieve a number of exact results which can be exploited as a guideline for the more complex PSW model.

C. Other limiting cases

In all previous cases, we have tacitly assumed $\epsilon_a > 0$. In principle, however, nothing prevents to consider the opposite case $\epsilon_a < 0$ (what implies $\gamma_a < 0$). In this case the PSW potential gives rise to an interesting class of

models, at least from an academic point of view, with two positive energy scales (ϵ_r and $|\epsilon_a|$). If $\epsilon_r > |\epsilon_a|$, we get a purely repulsive potential that could be called the penetrable square-shoulder (PSS) model (see Fig. 1). A peculiar situation occurs if $\epsilon_r < |\epsilon_a|$: when two particles approach they have first to overcome the barrier $|\epsilon_a|$ at $r = \sigma + \Delta$; once done, they feel an attractive well of depth $|\epsilon_a| - \epsilon_r$ for $r < \sigma$. Thus the potential is attractive for short distances and repulsive for larger distances. The simplest version of models with $\epsilon_a < 0$ and $\epsilon_r < |\epsilon_a|$ corresponds to $\epsilon_r = 0$, which will be referred to as the hollow penetrable-sphere (HPS) model (see Fig. 1). If, in addition, the limit $|\epsilon_a| \to \infty$ is taken, one gets an *athermal* potential that will be referred to as the hollow hard-sphere (HHS) model since the particles look like hard spheres of diameter $\sigma + \Delta$ with a "hole" of diameter σ inside. If two particles are separated by a distance larger than $\sigma + \Delta$, they behave as hard spheres and never know about their holes. On the other hand, if the separation between them is smaller than σ, they can never separate a distance larger than σ. In the HHS model, $\gamma_a \to -1$ and $\gamma_r \to 0$, so that the functions $y_2(r)$ and $g_2(r)$ are well defined (see below). In Section VI we will discuss the results for representative values of the parameters. A summary of the penetrable models treated in this paper, along with the corresponding values for the values for ϵ_r, ϵ_a, and Δ characterizing them, is reported in Table I.

III.   BASIC FORMALISM FOR EXACT PROPERTIES OF NEAREST-NEIGHBOR POTENTIALS

A.   General scheme

The great advantage of dealing with one-dimensional models is that they are usually amenable to exact solutions, at least in the limit of sufficiently short range interactions [14]. The trade-off is of course the fact that these models do not have phase transitions. In the context of fluids, this translates into the fact that there exist exact solutions for the HS, SHS, and SW models [5, 7, 8, 11, 13, 28, 29]. The same formalism allows one to tackle non-nearest-neighbor one-dimensional fluids [4] thus leading to an approximate solution. Let us recall the main results of this approach, referring to Ref. [13] for a self-contained treatment. The main quantity to be computed is the Laplace transform of the Boltzmann factor $e^{-\beta\phi(r)}$:

$$\widetilde{\Omega}(s) = \int_0^\infty ds \ e^{-sr} e^{-\beta\phi(r)}. \tag{3.1}$$

This is directly related to the Laplace transform of the radial distribution function $g(r)$,

$$\widetilde{G}(s) = \int_0^\infty ds \ e^{-sr} g(r), \tag{3.2}$$

where $\rho = N/L$ is the density of the one-dimensional fluid. The relation is (see Refs. [10, 13] for details)

$$\widetilde{G}(s) = \frac{1}{\rho} \left[\frac{\widetilde{\Omega}(\xi)}{\widetilde{\Omega}(s+\xi)} - 1 \right]^{-1}. \tag{3.3}$$

Here ξ is a solution of the equation

$$\left. \frac{\partial \ln \widetilde{\Omega}(s)}{\partial s} \right|_{s=\xi} = -\frac{1}{\rho}. \tag{3.4}$$

Finally, the equation of state (EOS) (and hence the whole thermodynamics) can be cast into the very simple form

$$\beta P = \xi, \tag{3.5}$$

where P is the pressure.

In practice, the scheme goes as follows. Evaluate $\widetilde{\Omega}(s)$ from the Boltzmann factor by a Laplace transform, Eq. (3.1); solve for ξ from Eq. (3.4); insert the result into Eq. (3.3); invert the Laplace transform (3.2) to obtain $g(r)$ and, in parallel, compute the EOS from (3.5).

As a final remark, we anticipate that, when dealing with discontinuous potentials (or Boltzmann factors), it is convenient to introduce the cavity function $y(r)$ which is related to the radial distribution function $g(r)$ and the pair potential $\phi(r)$ by the general relation

$$g(r) = e^{-\beta\phi(r)} y(r). \tag{3.6}$$

Moreover it can be expanded in powers of the density

$$y(r) = 1 + \sum_{n=1}^{\infty} \rho^n y_n(r).$$ (3.7)

In principle, the knowledge of all y_n coefficients provides the exact solution to the cavity function $y(r)$ (provided that the above series converges) and hence to the problem. This also allows us to assess the reliability of well known approximations involving the direct correlation function $c(r)$ and the cavity function [30], such as the Percus-Yevick (PY) closure

$$c(r) = f(r)y(r)$$ (3.8)

and the hypernetted chain (HNC) closure

$$c(r) = f(r)y(r) + y(r) - 1 - \ln y(r).$$ (3.9)

B. Exact solution of the SHS model in one dimension

Let us particularize the above procedure to derive the exact solution of Baxter's SHS model in one dimension. Starting from the Boltzmann factor

$$e^{-\beta\phi(r)} = \Theta(r - \sigma) + \alpha\sigma\delta_+(r - \sigma),$$ (3.10)

its Laplace transform (3.1) yields

$$\widetilde{\Omega}(s) = \left(\alpha\sigma + \frac{1}{s}\right)e^{-s\sigma}$$ (3.11)

Equation (3.4) can then be arranged to get the following quadratic equation

$$\xi^2\sigma^2\alpha(1 - \rho\sigma) + \xi\sigma(1 - \rho\sigma) - \rho\sigma = 0.$$ (3.12)

Its physical solution is

$$\xi = \frac{\sqrt{1 + 4\alpha\rho\sigma/(1 - \rho\sigma)} - 1}{2\alpha\sigma},$$ (3.13)

which can be substituted into Eq. (3.5) to give

$$\frac{\beta P}{\rho} = \frac{\sqrt{1 + 4\alpha\rho\sigma/(1 - \rho\sigma)} - 1}{2\alpha\rho\sigma},$$ (3.14)

which represents the EOS for this system. In order to get the exact radial distribution function, we exploit Eq. (3.3) to get

$$\widetilde{G}(s) = \frac{1}{\rho}\sum_{n=1}^{\infty}\left[\frac{\widetilde{\Omega}(s+\xi)}{\widetilde{\Omega}(\xi)}\right]^n$$

$$= \frac{1}{\rho}\sum_{n=1}^{\infty}\frac{\left(\alpha\sigma + \frac{1}{s+\xi}\right)^n e^{-ns\sigma}}{\left(\alpha\sigma + \frac{1}{\xi}\right)^n}.$$ (3.15)

We can now use the binomial theorem to expand $(\alpha\sigma + \frac{1}{s+\xi})^n$ and invert the Laplace transform (3.2) term by term by using the residue theorem, to obtain

$$g(r) = \sum_{n=1}^{\infty}\psi_n(r - n\sigma)\Theta(r - n\sigma),$$ (3.16)

$$\psi_n(r) = \frac{1}{\rho}\frac{1}{(\alpha\sigma + 1/\xi)^n}\left[(\alpha\sigma)^n\delta_+(r) + \sum_{k=1}^{n}\binom{n}{k}(\alpha\sigma)^{n-k}\frac{r^{k-1}e^{-\xi r}}{(k-1)!}\right],$$ (3.17)

which is the correct result found in Ref. [11] with a different method.

IV. EXACT PROPERTIES OF THE SPS MODEL

Next we turn our attention to the corresponding penetrable SPS counterpart. Following Ref. [4], the basic idea hinges on deducing the exact low-density orders of the SPS model from those of the SHS, which can be evaluated exactly. Each term $y_n(r)$ can be represented as a sum of suitable diagrams, whose forms for $y_1(r)$ and $y_2(r)$ were given in Ref. [4] and will not be repeated here. Each bond in the diagrams corresponds to a Mayer function $f(r)$ and the ones for the SPS and SHS models are related by Eq. (2.9). For the SHS model previously discussed, the exact cavity function $y(r)$ does not have a Dirac delta function at $r = \sigma$ and the regular part is continuous at that point. None of these two properties is any longer true for the SPS model, as further elaborated below. Here and in the following we set $\sigma = 1$ for simplicity.

The result is

$$y_1^{(\text{SPS})}(r) = \gamma_r^2 y_1^{(\text{SHS})}(r), \tag{4.1}$$

$$y_2^{(\text{SPS})}(r) = \gamma_r^3 y_{2A}^{(\text{SHS})}(r) + 2\gamma_r^4 y_{2B}^{(\text{SHS})}(r) + \frac{\gamma_r^4}{2} y_{2C}^{(\text{SHS})}(r) + \frac{\gamma_r^5}{2} y_{2D}^{(\text{SHS})}(r), \tag{4.2}$$

where the first-order density term is

$$y_1^{(\text{SHS})}(r) = (2 - r - 2\alpha)\,\Theta\,(2 - r) + \alpha^2\,[2\delta_+(r) + \delta_+(r - 2)]. \tag{4.3}$$

Note that this has a delta singularity at $r = 0$ and is continuous at $r = 1$. For the second order in density we have

$$
\begin{aligned}
y_{2A}^{(\text{SHS})}(r) &= \left[-\left(3 - r^2\right) + 6\alpha\,(1 - \alpha)\right]\Theta\,(1 - r) \\
&\quad + \left[-\frac{1}{2}\,(3 - r)^2 + 3\alpha\,(3 - \alpha - r)\right][\Theta\,(3 - r) - \Theta\,(1 - r)] \\
&\quad + \alpha^3\,[3\delta_+(r - 1) + \delta_+(r - 3)]\ ,
\end{aligned}
\tag{4.4}
$$

$$
\begin{aligned}
y_{2B}^{(\text{SHS})}(r) &= \left[\frac{1}{2}\,(6 - 2r - r^2) - \alpha\,(6 - 6\alpha - r)\right]\Theta\,(1 - r) \\
&\quad + \left[\frac{1}{2}\,(2 - r)\,(4 - r) - \alpha\,(8 - 4\alpha - 3r)\right][\Theta\,(2 - r) - \Theta\,(1 - r)] \\
&\quad + \alpha^2\,(1 - 2\alpha)\,[2\delta_+(r) + \delta_+(r - 2)] - 2\alpha^3\delta_+(r - 1)\ ,
\end{aligned}
\tag{4.5}
$$

$$y_{2C}^{(\text{SHS})}(r) = [y_1^{(\text{SHS})}(r)]^2\ , \tag{4.6}$$

$$
\begin{aligned}
y_{2D}^{(\text{SHS})}(r) &= [-(3 - 2r) + 2\alpha(3 - 3\alpha - r)]\Theta(1 - r) \\
&\quad + [-(2 - r)^2 + 4\alpha(2 - \alpha - r)][\Theta(2 - r) - \Theta(1 - r)] \\
&\quad + 2\alpha^3[6\delta_+(r) + \delta_+(r - 1) + 3\delta_+(r - 2)] - \alpha^4[4\delta_+^2(r) + \delta_+^2(r - 2)]\ .
\end{aligned}
\tag{4.7}
$$

The functions (4.4)–(4.7) present some peculiar properties. In particular, (i) the regular parts of $y_{2A}^{(\text{SHS})}(r)$, $y_{2B}^{(\text{SHS})}(r)$, and $y_{2D}^{(\text{SHS})}(r)$ are discontinuous at $r = 1$; (ii) $y_{2A}^{(\text{SHS})}(r)$, $y_{2B}^{(\text{SHS})}(r)$, and $y_{2D}^{(\text{SHS})}(r)$ have a delta singularity at $r = 1$; and (iii) $y_{2C}^{(\text{SHS})}(r)$ and $y_{2D}^{(\text{SHS})}(r)$ present delta-square singularities at $r = 0$ and $r = 2$. However, these three classes of singularities cancel out when setting $\gamma_r = 1$ in Eq. (4.2) to obtain the total second-order function $y_2^{(\text{SHS})}(r)$ [31]. On the other hand, since for SPS $y_{2A}^{(\text{SHS})}(r)$, $y_{2B}^{(\text{SHS})}(r)$, $y_{2C}^{(\text{SHS})}(r)$, and $y_{2D}^{(\text{SHS})}(r)$ are weighed by different powers of γ_r (3, 4, 4, and 5, respectively), the corresponding exact second-order cavity function is discontinuous at $r = 1$ and has a delta singularity at $r = 1$ and delta-square singularities at $r = 0$ and $r = 2$. The delta singularity at $r = 1$ is responsible for a diverging fourth virial coefficient of the SPS model (see below).

V. EXACT PROPERTIES OF THE PSW MODEL

A. Calculation of y_1 and y_2

As already mentioned, the SPS model suffers from the same drawbacks as the original SHS model plus some additional ones, so that it can hardly be regarded as a sound model in higher dimensions. However it has served as a test bench for analytical techniques. Armed by these tools we can now tackle the more difficult PSW model which has the SW fluid as a reference model. We recall that the latter does not have an exact solution in higher

dimensions but it is amenable to an exact treatment in one dimension [13]. The discussion follows closely the route already introduced for the SPS model, namely the density expansion, Eq. (3.7). The radial distribution function $g(r)$ is related to the cavity function $y(r)$ by Eq.(3.6) which with the help of Eqs. (2.2) and (2.3) yields

$$
g(r) = \begin{cases} (1 - \gamma_r) y(r), & r < 1, \\ (1 + \gamma\gamma_r) y(r), & 1 < r < 1 + \Delta, \\ y(r), & r > 1 + \Delta. \end{cases} \tag{5.1}
$$

As in the SPS model, the cavity function can be exactly computed up to second order in density, this time by reducing the problem to the solution of the SW model.

The first order term reads ($\Delta < 1$)

$$
y_1(r) = \gamma_r^2 \begin{cases} 2\left(1 + \gamma^2\Delta\right) - r\left(1 + 2\gamma + 2\gamma^2\right), & 0 \leq r \leq \Delta, \\ 2 - 2\gamma\Delta - r, & \Delta \leq r \leq 2, \\ \gamma(2 + \gamma)(r - 2) - 2\gamma\Delta, & 2 \leq r \leq 2 + \Delta, \\ (2 + 2\Delta - r)\gamma^2, & 2 + \Delta \leq r \leq 2 + 2\Delta, \\ 0, & 2 + 2\Delta \leq r. \end{cases} \tag{5.2}
$$

The second order can be reduced to the calculation of the corresponding diagrams of the SW model as anticipated. We find

$$
y_2(r) = \gamma_r^3 y_{2A}^{(SW)}(r) + 2\gamma_r^4 y_{2B}^{(SW)}(r) + \frac{\gamma_r^4}{2} y_{2C}^{(SW)}(r) + \frac{\gamma_r^5}{2} y_{2D}^{(SW)}, (r) \tag{5.3}
$$

where the explicit calculation of the various terms is described in Appendix B and is given by Eqs. (B1), (B2), (B4), and (B8). It can be checked that these expressions reduce to those of the SPS model, Eqs. (4.4)–(4.7), in the limit $\gamma \to \infty$ and $\Delta \to 0$ with $\alpha = \gamma\Delta/\sigma = \text{const.}$

B. Computation of B_2, B_3, and B_4

The EOS can be obtained from the knowledge of the radial distribution function $g(r)$ through a number of routes. The most common ones are the virial route

$$
\frac{\beta P}{\rho} \equiv Z(\rho, \beta) = 1 + 2^{d-1} v_d \rho \int_0^\infty dr \ r^d y(r) \frac{\partial}{\partial r} f(r), \tag{5.4}
$$

the compressibility route

$$
\left(\beta \frac{\partial P}{\partial \rho}\right)^{-1} \equiv \chi(\rho, \beta) = 1 + 2^d d v_d \rho \int_0^\infty dr \ r^{d-1} [g(r) - 1], \tag{5.5}
$$

and the energy route

$$
\frac{U}{N} \equiv u(\rho, \beta) = \frac{d}{2\beta} \left[1 + 2^d v_d \rho \beta \int_0^\infty dr \ r^{d-1} \phi(r) g(r)\right], \tag{5.6}
$$

where d is the dimensionality of the system and $v_d = (\pi/4)^{d/2}/\Gamma(1 + d/2)$ is the volume of a d-dimensional sphere of unit diameter. Thermodynamic consistency for the *exact* $g(r)$ requires the three routes to be completely equivalent and hence

$$
\chi^{-1}(\rho, \beta) = \frac{\partial}{\partial \rho} [\rho Z(\rho, \beta)], \tag{5.7}
$$

$$
\rho \frac{\partial}{\partial \rho} u(\rho, \beta) = \frac{\partial}{\partial \beta} Z(\rho, \beta). \tag{5.8}
$$

For an *approximate* $g(r)$, on the other hand, the consistency is no longer granted and different routes (or combinations of them) may lead to different results.

Let us specialize to the one-dimensional case of the PSW model, where we have just derived the exact $g(r)$ up to second order in a density expansion. Equations (5.4)–(5.6) become, using the potential (2.1),

$$Z\left(\rho,\beta\right) \;=\; 1 + \rho\gamma_r\left[\left(1+\gamma\right)y\left(1\right) - \gamma\left(1+\Delta\right)y\left(1+\Delta\right)\right], \tag{5.9}$$

$$\chi\left(\rho,\beta\right) \;=\; 1 + 2\rho\left\{\int_0^1 dr\;\left[\left(1-\gamma_r\right)y\left(r\right)-1\right] + \int_1^{1+\Delta} dr\;\left[\left(1+\gamma_r\gamma\right)y\left(r\right)-1\right] + \int_{1+\Delta}^{+\infty} dr\;\left[y\left(r\right)-1\right]\right\}, \tag{5.10}$$

$$u\left(\rho,\beta\right) \;=\; \frac{1}{2\beta} + \rho\left[\epsilon_r\left(1-\gamma_r\right)\int_0^1 dr\;y\left(r\right) - \epsilon_a\left(1+\gamma_r\gamma\right)\int_1^{1+\Delta} dr\;y\left(r\right)\right]. \tag{5.11}$$

Inserting the expansion (3.7) for the cavity function $y(r)$ we find

$$Z \;=\; 1 + B_2\rho + B_3\rho^2 + B_4\rho^3 + \cdots, \tag{5.12}$$

$$\chi \;=\; 1 + \chi_2\rho + \chi_3\rho^2 + \chi_4\rho^3 + \cdots, \tag{5.13}$$

$$u \;=\; \frac{1}{2\beta} + u_2\rho + u_3\rho^2 + u_4\rho^3 + \cdots. \tag{5.14}$$

Clearly Eq. (5.12) is the virial expansion for the compressibility factor Z whereas (5.13) and (5.14) are the analogous expansions for the isothermal compressibility χ and the energy per particle u. If the exact coefficients y_n appearing in Eq. (3.7) are known, the above three quantities provide the identical exact EOS.

On starting from the second-order values B_2, χ_2, and u_2 one can obtain perturbatively higher orders term by term from the knowledge of $y_n(r)$. The result can be cast into the form

$$B_2 \;=\; \gamma_r\left(1-\gamma\Delta\right), \quad \chi_2 = -2B_2, \quad u_2 = \epsilon_r\left(1-\gamma_r\right) - \epsilon_a\left(1+\gamma_r\gamma\right)\Delta, \tag{5.15}$$

$$B_n \;=\; \gamma_r\left[\left(1+\gamma\right)y_{n-2}\left(1\right) - \gamma\left(1+\Delta\right)y_{n-2}\left(1+\Delta\right)\right], \qquad n\geq 3, \tag{5.16}$$

$$\chi_n \;=\; 2\left[\left(1-\gamma\right)\int_0^1 dr\,y_{n-2}\left(r\right) + \left(1+\gamma_r\gamma\right)\int_1^{1+\Delta} dr\,y_{n-2}\left(r\right) + \int_{1+\Delta}^{\infty} dr\,y_{n-2}\left(r\right)\right], \qquad n\geq 3, \tag{5.17}$$

$$u_n \;=\; \epsilon_r\left(1-\gamma_r\right)\int_0^1 dr\,y_{n-2}\left(r\right) - \epsilon_a\left(1+\gamma_r\gamma\right)\int_1^{1+\Delta} dr\,y_{n-2}\left(r\right), \qquad n\geq 3. \tag{5.18}$$

Note that B_n depends upon y_{n-2} so that knowledge of the exact y_1 and y_2 allows the computation of the exact virial coefficients up to B_4. The third- and fourth-order results can be obtained from Eqs. (5.2) and (5.3). After some algebra, one gets

$$B_3 \;=\; \gamma_r^3\left[1 - \gamma\Delta\left(2-\Delta-2\gamma\Delta\right)\right], \tag{5.19}$$

$$\chi_3 \;=\; 4B_2^2 - 3B_3, \tag{5.20}$$

$$u_3 \;=\; \frac{\epsilon_r}{2}\gamma_r^2\left(1-\gamma_r\right)\left[3 - 2\gamma\Delta\left(2-\Delta-\gamma\Delta\right)\right] - \frac{\epsilon_a}{2}\gamma_r^2\left(1+\gamma_r\gamma\right)\Delta\left(2-\Delta-4\gamma\Delta\right)$$

$$\;=\; \frac{1}{2}\frac{\partial}{\partial\beta}B_3, \tag{5.21}$$

$$B_4 \;=\; -\frac{\gamma_r^6}{2}\left[1 - \gamma\Delta\left(3 - 3\Delta - 6\gamma\Delta + \Delta^2 + 4\gamma\Delta^2 + 3\gamma^2\Delta^2 - \gamma^3\Delta^2\right)\right]$$

$$\quad +\frac{\gamma_r^5}{2}\left[7 - \gamma\Delta\left(21 - 15\Delta - 36\gamma\Delta + 3\Delta^2 + 16\gamma\Delta^2 + 16\gamma^2\Delta^2 - 4\gamma^3\Delta^2\right)\right]$$

$$\quad -\frac{\gamma_r^4}{2}\left[4 - \gamma\Delta\left(12 - 6\Delta - 18\gamma\Delta + \Delta^2 + 3\gamma\Delta^2 + 3\gamma^2\Delta^2 - 3\gamma^3\Delta^2\right)\right], \tag{5.22}$$

$$\chi_4 \;=\; -4\left(2B_2^3 - 3B_2B_3 + B_4\right), \tag{5.23}$$

$$u_4 \;=\; \frac{1}{3}\frac{\partial}{\partial\beta}B_4. \tag{5.24}$$

The three routes provide consistently identical results for B_3 and B_4, i.e., the relations (5.7) and (5.8) are verified, as they should. In the energy case the following identity is needed:

$$\frac{\partial}{\partial\beta} \;=\; \frac{\partial\gamma_r}{\partial\beta}\frac{\partial}{\partial\gamma_r} + \frac{\partial\gamma}{\partial\beta}\frac{\partial}{\partial\gamma}$$

$$\;=\; \epsilon_r\left(1-\gamma_r\right)\frac{\partial}{\partial\gamma_r} + \frac{\epsilon_a\left(1+\gamma_r\gamma\right) - \epsilon_r\gamma\left(1-\gamma_r\right)}{\gamma_r}\frac{\partial}{\partial\gamma}. \tag{5.25}$$

Equation (5.22) gives the exact fourth virial coefficient as a function of the three relevant parameters of the PSW model, namely γ_r, γ, and Δ. The results for the PS and SW models are recovered as

$$\lim_{\epsilon_a \to 0} B_4 = \lim_{\epsilon_a \to -\epsilon_r} \frac{B_4}{(1+\Delta)^3} = \gamma_r^4 \left(-\frac{\gamma_r^2}{2} + \frac{7\gamma_r}{2} - 2\right), \tag{5.26}$$

$$\lim_{\epsilon_r \to \infty} B_4 = 1 - \gamma\Delta \left(3 - 3\Delta - 6\gamma\Delta + \frac{1}{2}\Delta^2 + \frac{9}{2}\gamma\Delta^2 + 5\gamma^2\Delta^2\right), \tag{5.27}$$

respectively. On the other hand, while B_2 and B_3 are well defined in the SPS limit ($\gamma \to \infty$ and $\Delta \to 0$ with $\alpha = \gamma\Delta = $ finite) [see Eqs. (5.15) and (5.19)], the presence of the terms $\gamma^3\Delta^2$ in Eq. (5.22) implies that $B_4 \to \infty$ in the SPS model. Equation (5.16) shows that this is a direct consequence of the divergence of $y_2^{(\mathrm{SPS})}(r)$ at $r = 1$. However, $y_2^{(\mathrm{SHS})}(1) = $ finite, so that B_4 is well defined in the SHS model ($\gamma_r = 1$), as shown by Eq. (5.27).

The second, third, and fourth virial coefficients for the PSS model ($\epsilon_a < 0$) are still given by Eqs. (5.15), (5.19), and (5.22), except that $\gamma < 0$. In the case of the HPS model ($\epsilon_a < 0$ and $\epsilon_r \to 0$ or, equivalently, $\gamma_a < 0$, $\gamma = \gamma_a/\gamma_r$, and $\gamma_r \to 0$), one gets

$$\lim_{\epsilon_r \to 0} B_2 = -\gamma_a\Delta, \quad \lim_{\epsilon_r \to 0} B_3 = 0, \quad \lim_{\epsilon_r \to 0} B_4 = -\frac{3}{2}\gamma_a^4\Delta^3. \tag{5.28}$$

The special case of the HHS model is obtained by further taking the limit $\epsilon_a \to \infty$ ($\gamma_a \to -1$).

VI. SOME ILLUSTRATIVE CASES AND COMPARISON WITH THE PY AND HNC APPROXIMATIONS

The approximate character of a given closure can be typically inferred by looking at $g_2(r)$ along with the corresponding fourth virial coefficient B_4. Being coefficients in a density expansion, both can be either positive or negative. We now plot the exact $g_2(r)$ and B_4 for some illustrative cases and compare them with the PY and HNC theories (3.8) and (3.9). The PY and HNC results corresponding to Eq. (5.3) are [30]

$$y_2^{\mathrm{PY}}(r) = \gamma_r^3 y_{2A}^{(\mathrm{SW})}(r) + 2\gamma_r^4 y_{2B}^{(\mathrm{SW})}(r), \tag{6.1}$$

$$y_2^{\mathrm{HNC}}(r) = \gamma_r^3 y_{2A}^{(\mathrm{SW})}(r) + 2\gamma_r^4 y_{2B}^{(\mathrm{SW})}(r) + \frac{\gamma_r^4}{2} y_{2C}^{(\mathrm{SW})}(r). \tag{6.2}$$

Comparison with Eq. (5.3) shows that the HNC theory neglects $y_{2D}^{(\mathrm{SW})}(r)$ and the PY theory neglects, in addition, $y_{2C}^{(\mathrm{SW})}(r)$. As a consequence, the expression for the fourth virial coefficient in the PY and HNC approximations depends on the thermodynamic route. The corresponding results can be found in Appendix C.

Let us start with $g_2(r)$. As a prototypical PSW system we have chosen $\epsilon_a/\epsilon_r = 0.25$ and $\Delta = 0.5$. Figure 2 shows $g_2(r)$ for $k_BT/\epsilon_r = 0.5$ and $k_BT/\epsilon_r = 1$. It can be observed that the HNC and PY tend to overestimate and underestimate, respectively, the values of $g_2(r)$ in the overlapping region $r < 1$. This is due to the fact that $y_{2D}^{(\mathrm{SW})}(r)$ is generally negative in the region $r < 1$, while $y_{2C}^{(\mathrm{SW})}(r)$ is positive definite and larger than the magnitude of $y_{2D}^{(\mathrm{SW})}(r)$. Inside the well ($1 < r < 1 + \Delta$) the PY and HNC curves practically coincide at $k_BT/\epsilon_r = 0.5$, both being rather inaccurate, while at the higher temperature $k_BT/\epsilon_r = 1$ the PY prediction is quite good. Moreover, the PY theory is a better approximation than the HNC theory for $r > 2$. This is explained by the fact that $y_{2C}^{(\mathrm{SW})}(r) + y_{2D}^{(\mathrm{SW})}(r) = 0$ in the region $r > 2$, so that $g_2^{\mathrm{PY}}(r)$ coincides with the exact $g_2(r)$ for $r > 2$ in the case of the SW model ($\gamma_r = 1$). If $\gamma_r < 1$ the combination $y_{2C}^{(\mathrm{SW})}(r) + \gamma_r y_{2D}^{(\mathrm{SW})}(r)$ does not vanish for $r > 2$ but is still rather small for the cases of Fig. 2. For $r > 2 + 2\Delta$, both $g_2^{\mathrm{HNC}}(r)$ and $g_2^{\mathrm{PY}}(r)$ become exact since $y_{2C}^{(\mathrm{SW})}(r)$ and $y_{2D}^{(\mathrm{SW})}(r)$ vanish in that region.

Figure 3 depicts the function $g_2(r)$ for a representative case of the PSS model (see Section II C). Most of the preceding comments in connection with Fig. 2 apply here as well. Finally, the function $g_2(r)$ corresponding to the HPS model is shown in Fig. 4 for $\Delta = 0.5$ and two temperatures: $k_BT/|\epsilon_a| = 0$ and $k_BT/|\epsilon_a| = 0.5$. Note that the zero-temperature case is equivalent to the HHS limit. It is interesting to note that the curves corresponding to both temperatures are quite similar, except for a change of scale. In the HPS model the HNC theory gives the exact $g_2(r)$ because, for large $|\gamma|$, $y_{2D}^{(\mathrm{SW})}(r)$ scales with γ^4, while it has a weight γ_r^5 and so does not contributes to $y_2(r)$. Similarly,
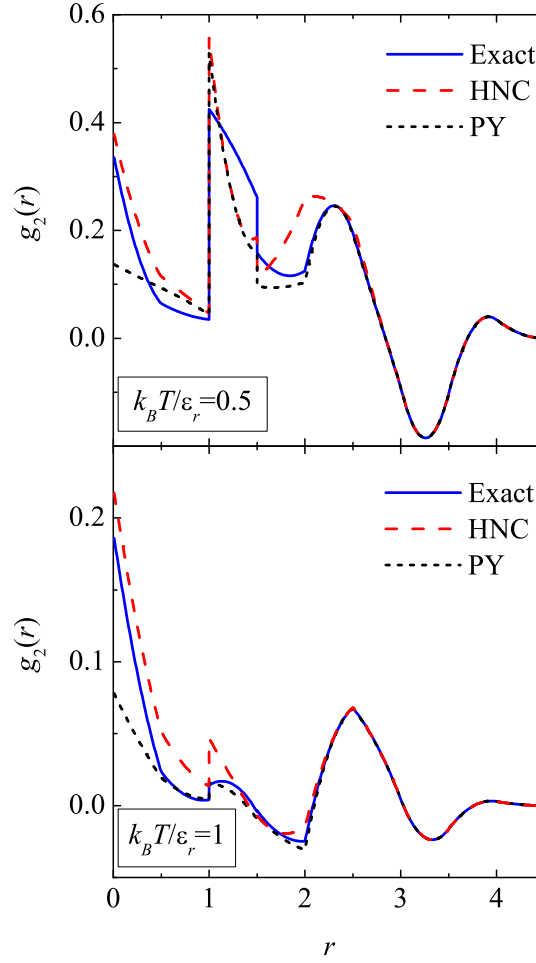
FIG. 2: (Color online) Plot of the second-order radial distribution function, $g_2(r)$, for a PSW model with $\epsilon_a/\epsilon_r = 0.25$, $\Delta = 0.5$, and $k_B T/\epsilon_r = 0.5$ (top panel) and $k_B T/\epsilon_r = 1$ (bottom panel). The solid, long-dashed, and short-dashed lines correspond to the exact result, the HNC approximation, and the PY approximation, respectively.

$y_{2B}^{(\mathrm{SW})}(r)$ scales with γ^3 and so it does not contribute to $y_2(r)$ either. On the other hand, $\gamma_r^4 y_{2C}^{(\mathrm{SW})}(r)$ is different from zero in the regions $0 \leq r \leq \Delta$ and $2 \leq r \leq 2 + 2\Delta$ and it is there where the PY theory fails, yielding $g_2^{\mathrm{PY}}(r) = 0$.

In order to have a feeling of the behavior of the exact B_4, we now plot them for some representative values of the parameters. Figure 5 shows the exact [see Eq. (5.22)] and the approximate (see Appendix C) values of the fourth virial coefficient as functions of temperature for the same PSW model as considered in Fig. 2, i.e., the one defined by $\epsilon_a/\epsilon_r = 0.25$ and $\Delta = 0.5$. While the exact B_4 goes to $-\infty$ as $T \to 0$, the HNC and PY theories artificially predict a divergence to $+\infty$. We can observe that the best agreement with the exact curve corresponds to $B_4^{\mathrm{HNC},c}$ up to $k_B T/\epsilon_r \simeq 0.5$ and to $B_4^{\mathrm{PY},c}$ thereafter. The worst behaviors correspond to $B_4^{\mathrm{HNC},v} = B_4^{\mathrm{HNC},e}$ and $B_4^{\mathrm{PY},v}$.

The results for the PSS model considered in Fig. 3, namely $\epsilon_a/\epsilon_r = -0.5$ and $\Delta = 0.5$, are displayed in Fig. 6. For low temperatures this model reduces to the HS model of diameter $1 + \Delta$. It is found that $B_4^{\mathrm{PY},v}$ and, especially, $B_4^{\mathrm{PY},c}$ present an excellent agreement with the exact B_4. On the other hand, the poorest performances are presented by $B_4^{\mathrm{HNC},v} = B_4^{\mathrm{HNC},e}$ and $B_4^{\mathrm{PY},e}$.

We have also evaluated B_4 for the HPS model at various values of $k_B T/|\epsilon_a|$, as depicted in Fig. 7, and compared with the PY approximation (compressibility route). As said before, the HNC theory becomes exact for the HPS model. Interestingly, in this case both the virial and the energy routes from the PY approximation yield exact results, even though $y_2^{\mathrm{PY}}(r)$ is not exact.

It is worthwhile noting that B_4 is not a monotonic function of temperature in the PSW model (see Fig. 5): it is negative for low temperatures, reaches a positive maximum value at an intermediate temperature, and then decays, reaching a very small negative minimum value at a certain temperature, and finally going to zero from below. Although hardly apparent in Fig. 6, the behavior of B_4 is also non-monotonic in the PSS model: it is generally positive and
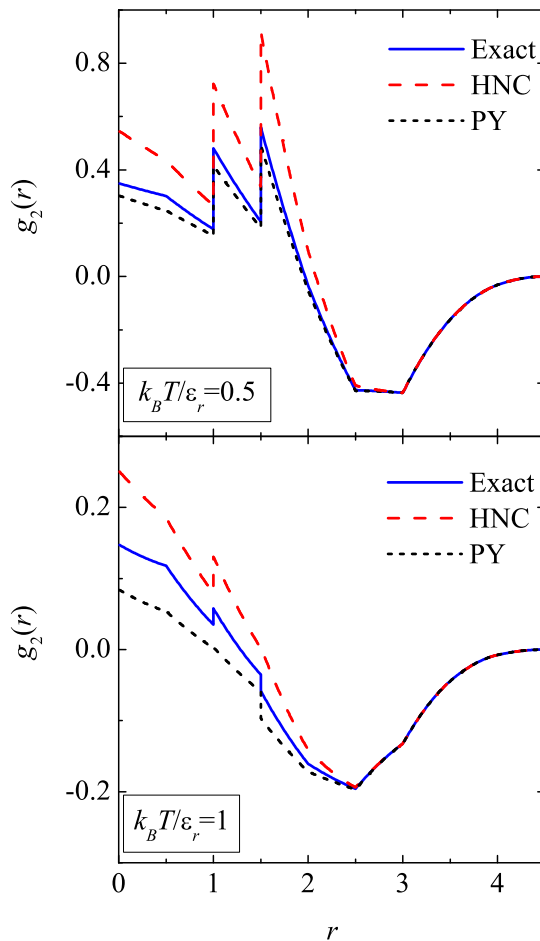
FIG. 3: (Color online) Plot of the second-order radial distribution function, $g_2(r)$, for a PSS model with $\epsilon_a/\epsilon_r = -0.5$, $\Delta = 0.5$, and $k_B T/\epsilon_r = 0.5$ (top panel) and $k_B T/\epsilon_r = 1$ (bottom panel). The solid, long-dashed, and short-dashed lines correspond to the exact result, the HNC approximation, and the PY approximation, respectively.

decays as the temperature increases, but eventually reaches a very small negative minimum value and thereafter tends to zero from below. In contrast, the fourth virial coefficient of the HPS model (see Fig. 7) is negative definite and monotonically increases with increasing temperature.

VII. CONCLUSIONS AND OUTLOOK

In this paper, we have introduced the PSW model and outlined a number of exact results for this model in one dimension. The potential contains two energy scales (the core barrier ϵ_r and the well depth ϵ_a) and two length scales (the core diameter σ and the well width Δ). This model is a variation of the widely used square-well one with a finite energy barrier replacing the hard core. As such, this is not a nearest-neighbor system and there exists no general approach leading to an exact solution even in the one-dimensional case. In spite of this we have been able to obtain the exact first few coefficients in the density expansions of the relevant structural and thermodynamical properties. Specifically, we have computed both the cavity and radial distribution functions up to second order in density and the virial expansion up to fourth order. As a stringent test of the calculations, we have explicitly checked that different routes to thermodynamics (virial, compressibility, and energy) are consistent one another up to this order.

This model includes a variety of other models as special cases. By taking the limit of infinitely narrow and deep well ($\epsilon_a \to \infty$, $\Delta \to 0$) we obtain the SPS model which can be also reckoned as a variant of the SHS model with penetrable core. Upon reversing the sign of the attractive energy scale ϵ_a we obtain a PSS model with successive soft repulsive barriers of decreasing height. If the second barrier is higher that the first ($-\epsilon_a > \epsilon_r > 0$), we find a potential that is attractive for short distances and repulsive for larger distances. An interesting situation, that we have denoted as HPS, corresponds to $-\epsilon_a > \epsilon_r = 0$. In the limit of zero temperature (or, equivalently, $\epsilon_a \to -\infty$)
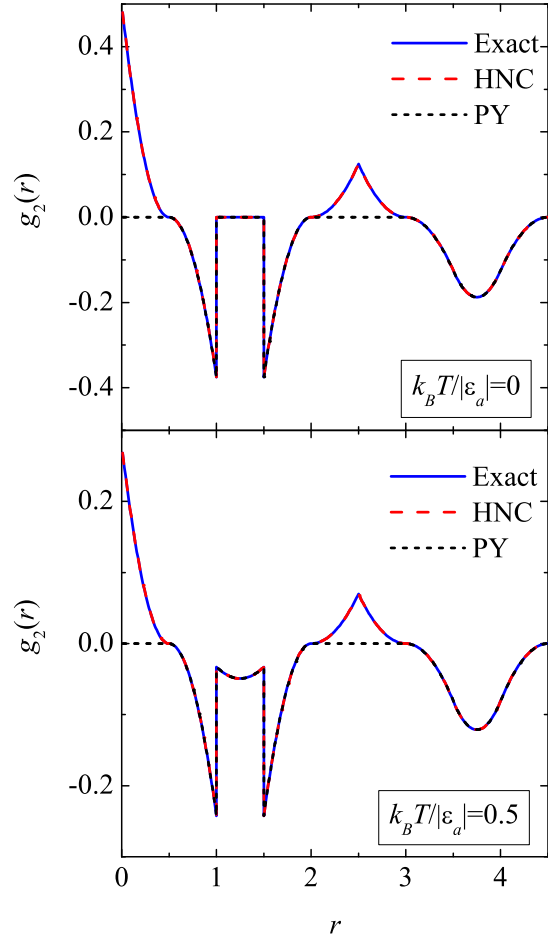
FIG. 4: (Color online) Plot of the second-order radial distribution function, $g_2(r)$, for the HPS model with $\Delta = 0.5$ and $k_B T/|\epsilon_a| = 0.5$ (bottom panel) and $k_B T/|\epsilon_a| = 0$ (top panel, corresponding to the HHS model). The solid, long-dashed, and short-dashed lines correspond to the exact result, the HNC approximation, and the PY approximation, respectively. Note that the HNC approximation provides the exact result in the HPS model.
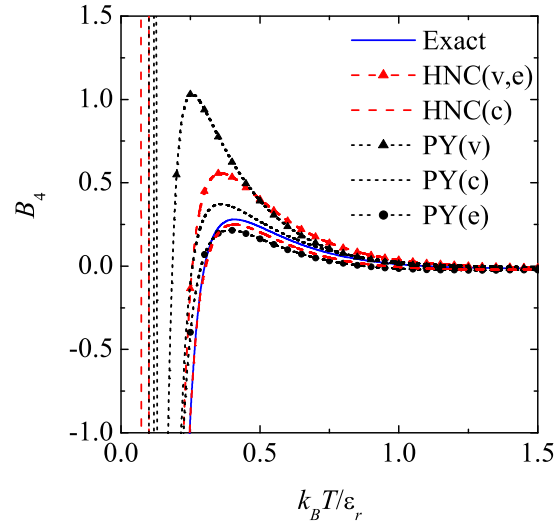

FIG. 5: (Color online) Plot of the fourth virial coefficient, B_4, as a function of $k_B T/\epsilon_r$ for a PSW model with $\epsilon_a/\epsilon_r = 0.25$ and $\Delta = 0.5$. The solid, dashed, and dotted lines correspond to the exact result, the HNC approximation (virial/energy and compressibility routes), and the PY approximation (virial, compressibility, and energy routes), respectively.

FIG. 6: (Color online) Plot of the fourth virial coefficient, B_4, as a function of $k_B T/\epsilon_r$ for a PSS model with $\epsilon_a/\epsilon_r = -0.5$ and $\Delta = 0.5$. The solid, dashed, and dotted lines correspond to the exact result, the HNC approximation (virial/energy and compressibility routes), and the PY approximation (virial, compressibility, and energy routes), respectively.
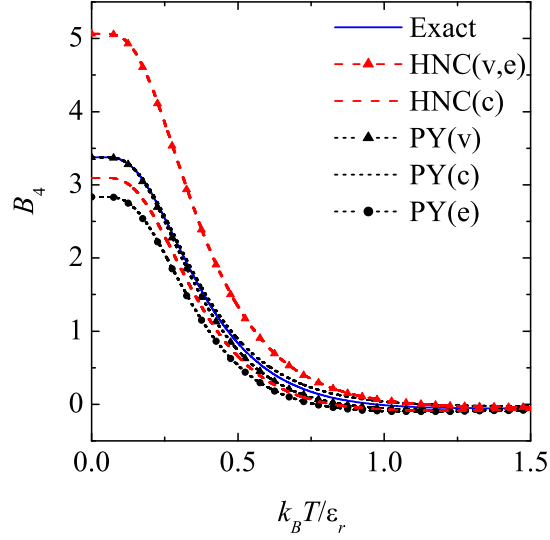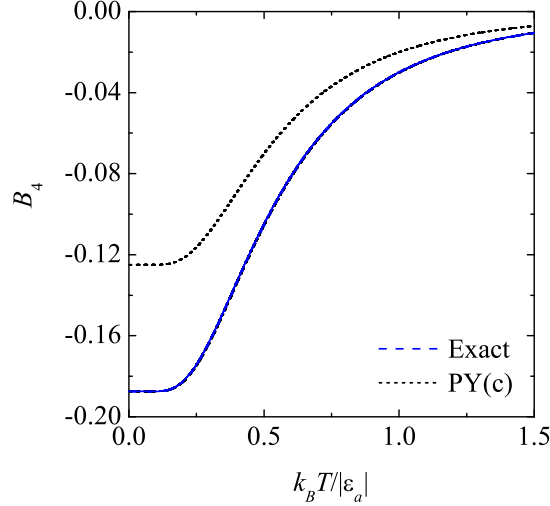

FIG. 7: (Color online) Plot of the fourth virial coefficient, B_4, as a function of $k_B T/|\epsilon_a|$ for a HPS model with $\Delta = 0.5$. The dashed line corresponds to the exact result whereas the dotted line correspond to the PY approximation (compressibility route).

the HPS model becomes the HHS model, characterized by an infinitely high barrier between σ and $\sigma + \Delta$. Here the equilibrium state consists of "chains" of connected particles: two adjacent particles of the same chain move freely, provided that the distance between their centers does not exceed σ; on the other hand, particles of different chains behave as hard spheres of diameter $\sigma + \Delta$. In the limit $|\epsilon_a| \to 0$ (and also if $-\epsilon_a = \epsilon_r > 0$) the PSW fluid reduces to the PS one, and all results obtained here are consistent with previous analysis on the PS model within this limit. Finally, all results smoothly converge to the HS limit when $\epsilon_r \to \infty$ and $|\epsilon_a| \to 0$ (or $-\epsilon_a = \epsilon_r \to \infty$), as expected.

The combined effect of the absence of a hard core and the presence of a finite attractive part of the PSW potential raises the issue of the existence of a well-defined thermodynamic limit of the system. We have analyzed this issue in detail and we have assessed the limits of stability as a function of the ratio between the attractive and repulsive energy scales: when $\epsilon_a/\epsilon_r \leq \frac{1}{2}$ the system is stable whereas in the opposite case the system might be unstable (when $\epsilon_r > 0$ and $\epsilon_a < 0$ the system is always stable independently of the energy scales). The SPS limit turns out to be always unstable since the exact fourth-order virial coefficient diverges, unlike the corresponding SHS counterpart which is well-behaving.

A main advantage of exact relations is that one can asses the reliability of approximate theories. A comparison with PY and HNC closures unveils the corresponding strengths and weaknesses of both. We have found that each of them has a domain in space where it outperforms the other, and we have explained why this is so in terms of the exact and approximate behavior of the second-order cavity function $y_2(r)$. As a general feature, HNC tends to overestimate the cavity function within the core whereas PY has the opposite tendency. On the other hand, PY is consistently superior in the large-r region. Both approximate theories produce artifacts in the low temperature region of the fourth virial coefficients.

It would be extremely interesting to extend the present work in some respects. While our analysis has provided a careful comparison of the PY and HNC approximate theories with respect to the exact result, we have not attempted a detailed physical interpretation of the results. This is because our exact analysis was limited to the lowest orders in density, which are expected to be valid only within a rather limited region of the phase diagram. It turns out, however, that even this limited knowledge can be exploited to construct rather precise approximations for the PSW model in the limits of small penetrability $(1 - \gamma_r \ll 1)$ and high penetrability $(\gamma_r \ll 1)$, for arbitrary value of the density. This analysis mirrors that already performed for the PS model [4, 17], can be tested against numerical simulations, and nicely complements the exact low-density results presented here. The boundedness of the class of penetrable-sphere potentials raises the possibility of a phase transition even in a one-dimensional system [32, 33] and the presence of the attractive part might also give rise to additional transitions in the fluid phase. We plan to address this point in future work.

It is worth stressing that the large number of parameters present in the PSW fluid (two energy scales, two characteristic lengths, density, and temperature) may render the phase diagram analysis quite problematic, so an exact understanding of the low-dimensional behavior, where the analysis can be carried out almost fully analytically, is always welcome. Having done this, the extension to three dimensions should be facilitated, and our results predict an extremely rich phase diagram which might be useful to describe complex fluids with soft cores within a unified picture.

APPENDIX A: RUELLE'S STABILITY CRITERION

According to Ruelle's criterion, a sufficient condition of thermodynamic stability is [18, 19]

$$U_N(x_1, \ldots, x_N) = \sum_{i=1}^{N-1} \sum_{j=i+1}^{N} \phi(|x_i - x_j|) \geq -NB \tag{A1}$$

for all configurations $\{x_i\}$, where B is a fixed bound.

Let us first demonstrate that for small repulsion $(\epsilon_r < 2\epsilon_a)$ there exists at least one configuration violating the stability constraint. We consider a particular configuration where the N particles are distributed into N/s overlapping clusters of s particles each, so that the centers of the s particles belonging to the same cluster coincide (with a tolerance $\Delta/2$). Next, the centers of two adjacent clusters are separated by a distance between σ and $\sigma + \Delta$. The potential energy corresponding to this configuration is

$$U_N(s) = \frac{N}{s} \frac{s(s-1)}{2} \epsilon_r - \left(\frac{N}{s} - 1\right) s^2 \epsilon_a , \tag{A2}$$

The first term on the right-hand side represents the repulsive energy of the $s(s-1)/2$ pairs of each cluster, times the number of clusters. The second term is the attractive energy of the interaction between the s particles of each cluster and the s particles of its neighbor cluster, times the number of pairs of adjacent clusters. Obviously, the value of the total potential energy U_N depends on the value of s. The extreme cases are $s = 1$ and $s = N$. We then see that the value that minimizes $U_N(s)$ is

$$s_* = \frac{N}{2} \left(1 - \frac{\epsilon_r}{2\epsilon_a}\right) , \tag{A3}$$

which is meaningful only if $\epsilon_r < 2\epsilon_a$. The corresponding minimum value of $U_N(s)$ is

$$U_N(s_*) = -N \left[\frac{\epsilon_r}{2} + \frac{N}{16} \epsilon_a \left(2 - \frac{\epsilon_r}{\epsilon_a}\right)^2\right] , \quad \epsilon_r < 2\epsilon_a . \tag{A4}$$

The quantity enclosed between brackets grows linearly with N and so it is not bounded. Therefore, if $\epsilon_r < 2\epsilon_a$, there exists at least a configuration that violates Ruelle's criterion. On the other hand, we note that if $\epsilon_r > 2\epsilon_a$ the

minimum of $U_N(s)$ is reached at $s = 1$, in which case

$$U_N(s) \geq U_N(s = 1) = -(N - 1)\epsilon_a , \quad \epsilon_r > 2\epsilon_a , \tag{A5}$$

so that all these special configurations are consistent with Ruelle's criterion. Indeed we now show that no other configurations violate Ruelle's criterion if $\epsilon_r > 2\epsilon_a$ so that the model is thermodynamically stable if the above condition is satisfied.

Without loss of generality we can see any given configuration of N particles as a set of M clusters ($1 \leq M \leq N$), each cluster i being made of s_i *overlapping* particles (i.e., any pair of particles of a given cluster are separated a distance smaller than σ). For fixed M and $\{s_i\}$, the total potential energy can be decomposed as

$$U_N(\{s_i\}; M) = U_N^{\text{intra}}(\{s_i\}; M) + U_N^{\text{inter}}(\{s_i\}; M), \tag{A6}$$

where

$$U_N^{\text{intra}}(\{s_i\}; M) = \frac{\epsilon_r}{2} \sum_{i=1}^{M} s_i(s_i - 1) \tag{A7}$$

is the contribution associated with pairs of particles inside each cluster and U_N^{inter} is the contribution associated with pairs of particles belonging in different clusters. Note that in the latter contribution the energy for each pair can be ϵ_r (if the separation is smaller than σ), $-\epsilon_a$ (if the separation lies between σ and $\sigma + \Delta$), or zero (if the separation is larger than $\sigma + \Delta$). It is clear that the minimum value of U_N^{inter} is achieved when all the particles of a cluster interact attractively with all the particles of the neighbor cluster:

$$U_N^{\text{inter}}(\{s_i\}; M) \geq -\epsilon_a \sum_{i=1}^{M-1} s_i s_{i+1} > -\epsilon_a \sum_{i=1}^{M-1} s_i s_{i+1} - \epsilon_a s_1 s_M . \tag{A8}$$

Therefore,

$$U_N(\{s_i\}; M) > \frac{\epsilon_r}{2} \sum_{i=1}^{M} s_i(s_i - 1) - \frac{\epsilon_a}{2} \sum_{i=1}^{M} s_i(s_{i-1} + s_{i+1}) \equiv W_N(\{s_i\}; M) , \tag{A9}$$

where $s_0 = s_M$ and $s_{M+1} = s_1$. Given M, what is the set of population numbers $\{s_i\}$ that minimizes W_N subject to the constraint that $\sum_{i=1}^{M} s_i = N$? Using a Lagrange multiplier λ, the problem reduces to solve

$$\frac{\partial}{\partial s_j} \left[W_N(\{s_i\}; M) - \lambda \sum_{i=1}^{M} s_i \right] = \frac{\epsilon_r}{2}(2s_j - 1) - \epsilon_a(s_{j-1} + s_{j+1}) - \lambda = 0 , \quad 1 \leq j \leq M . \tag{A10}$$

The solution is $s_i = N/M$ and $\lambda = (N/M)(\epsilon_r - 2\epsilon_a) - \epsilon_r/2$. This could have been expected by symmetry arguments. Therefore, given M clusters, the minimum W_N is obtained with a uniform distribution $s_i = s = N/M$. For $\epsilon_r > 2\epsilon_a$ we can thus write

$$U_N(\{s_i\}; M) > W_N(\{s_i = N/M\}; M) = \frac{\epsilon_r}{2}M(N/M)(N/M - 1) - \epsilon_a M(N/M)^2$$
$$= (\epsilon_r/2 - \epsilon_a)N^2/M - N\epsilon_r/2 > -N\epsilon_r/2 , \tag{A11}$$

which proves that Ruelle's stability criterion is satisfied.

APPENDIX B: SECOND-ORDER CAVITY FUNCTIONS FOR SW

The first-order term $y_1^{(\text{SW})}(r)$ (for $\Delta < \sigma \equiv 1$) is given by Eq. (5.2) with $\gamma_r = 1$. This allows for a straightforward determination of $y_{2C}^{(\text{SW})}(r)$ as

$$y_{2C}^{(\text{SW})}(r) = \left[y_1^{(\text{SW})}(r) \right]^2 . \tag{B1}$$

Next, one can also evaluate the Fourier transform of the integral corresponding to the $2A$ diagram. Going back to real space, the result is

$$
\begin{aligned}
y_{2A}^{(\text{SW})}(r) \;=\; & -\frac{3}{2}\gamma\,(1+\gamma)^2\,(1-\Delta-r)^2\,\Theta\,(1-\Delta-r) + \frac{3}{2}\,(1+\gamma)\,(1+2\gamma+3\gamma^2)\,(1-r)^2\,\Theta\,(1-r) \\
& -\frac{3}{2}\gamma\,(2+4\gamma+3\gamma^2)\,(1+\Delta-r)^2\,\Theta\,(1+\Delta-r) + \frac{3}{2}\gamma^2\,(1+\gamma)\,(1+2\Delta-r)^2\,\Theta\,(1+2\Delta-r) \\
& -\frac{1}{2}\,(1+\gamma)^3\,(3-r)^2\,\Theta\,(3-r) + \frac{3}{2}\gamma\,(1+\gamma)^2\,(3+\Delta-r)^2\,\Theta\,(3+\Delta-r) \\
& -\frac{3}{2}\gamma^2\,(1+\gamma)\,(3+2\Delta-r)^2\,\Theta\,(3+2\Delta-r) + \frac{1}{2}\gamma^3\,(3+3\Delta-r)^2\,\Theta\,(3+3\Delta-r)\,.
\end{aligned}
\tag{B2}
$$

For $y_{2B}^{(\text{SW})}(r)$ we can make use of the identity

$$
y_{2B}(r) \;=\; \int_{-\infty}^{\infty} ds\; y_1(s)\, f(s)\, f(|r-s|)\,,
\tag{B3}
$$

which leads to the result

$$
\begin{aligned}
y_{2B}^{(\text{SW})}(r) \;=\; & \gamma\,(1+\gamma)\,(2-\Delta-4\gamma\Delta)\,(\Delta-r)\,\Theta\,(\Delta-r) + \gamma\,(1+\gamma)^2\,(1-\Delta-r)^2\,\Theta\,(1-\Delta-r) \\
& -\left(1+3\gamma+5\gamma^2+3\gamma^3\right)(1-r)^2\,\Theta\,(1-r) + \gamma\,(2+4\gamma+3\gamma^2)\,(1+\Delta-r)^2\,\Theta\,(1+\Delta-r) \\
& -\gamma^2\,(1+\gamma)\,(1+2\Delta-r)^2\,\Theta\,(1+2\Delta-r) + \frac{1}{2}\,(1+\gamma)^2\,(4-r-4\gamma\Delta)\,(2-r)\,\Theta\,(2-r) \\
& -\gamma\,(1+\gamma)\,(4-r-4\gamma\Delta)\,(2+\Delta-r)\,\Theta\,(2+\Delta-r) + \frac{1}{2}\gamma^2\,(4-r-4\gamma\Delta)\,(2+2\Delta-r)\,\Theta\,(2+2\Delta-r)\,.
\end{aligned}
\tag{B4}
$$

Computation of $y_{2D}^{(\text{SW})}(r)$ is much more laborious and requires a different route. We go back to the general formalism and compute the exact $\widetilde{\Omega}(s)$ from the Laplace transform (3.1), which is

$$
\widetilde{\Omega}(s) \;=\; \frac{e^{-s}}{s}\left(1+\gamma-\gamma e^{-s\Delta}\right).
\tag{B5}
$$

Equation (3.4) then yields for the parameter ξ the following density expansion:

$$
\xi \;=\; \rho + (1-\gamma\Delta)\,\rho^2 + \left[1-\gamma\Delta\,(2-\Delta-2\gamma\Delta)\right]\rho^3 + \cdots\,.
\tag{B6}
$$

Inserting this solution into Eq. (3.3) and inverting the Laplace transform (3.2), we can obtain the corresponding radial distribution function $g_2(r)$ correct up to second order in density. Use of Eq. (5.1) then yields the corresponding cavity function $y_2(r)$ and then $y_{2D}^{(\text{SW})}(r)$ is given by the difference

$$
y_{2D}^{(\text{SW})}(r) \;=\; 2y_2(r) - 2y_{2A}^{(\text{SW})}(r) - 4y_{2B}^{(\text{SW})}(r) - 4y_{2C}^{(\text{SW})}(r)\,.
\tag{B7}
$$

This provides the result for $r \geq 1$. Inside the core we have three different regions under the assumption that $\Delta \leq 1$, namely $0 \leq r \leq \Delta$, $\Delta \leq r \leq 1-\Delta$ and $1-\Delta \leq r \leq 1$. The quadratic expression in each region can be obtained by imposing continuity conditions and with some help from numerical evaluation. The final analytic result is

$$
\begin{aligned}
y_{2D}^{(\text{SW})}(r) \;=\; & -2\gamma\,(1+\gamma)\left[(1+\gamma+\gamma^2)\,r - 2 + \Delta\,(1+3\gamma-\gamma^2)\right](\Delta-r)\,\Theta\,(\Delta-r) \\
& -\gamma\,(1+\gamma)^2\,(1-\Delta-r)^2\,\Theta\,(1-\Delta-r) + \left(1+3\gamma+5\gamma^2+3\gamma^3\right)(1-r)^2\,\Theta\,(1-r) \\
& -\gamma\,(2+4\gamma+3\gamma^2)\,(1+\Delta-r)^2\,\Theta\,(1+\Delta-r) + \gamma^2\,(1+\gamma)\,(1+2\Delta-r)^2\,\Theta\,(1+2\Delta-r) \\
& +(1+\gamma)^2\left[r\,(1-2\gamma-\gamma^2) - 2 + 4\gamma + 2\gamma^2 + 4\gamma\Delta\right](2-r)\,\Theta\,(2-r) \\
& +4\gamma^2\,(1+\gamma)\,(r-2-\Delta+\gamma\Delta)\,(2+\Delta-r)\,\Theta\,(2+\Delta-r) - \gamma^4\,(2+2\Delta-r)^2\,\Theta\,(2+2\Delta-r)\,. \quad \text{(B8)}
\end{aligned}
$$

Note that the first derivative $y'(r)$ is discontinuous at $r = \Delta$, 2, $2+\Delta$, and $2+2\Delta$, as it can be inferred from its explicit computation at this order in density.

APPENDIX C: CALCULATION OF B_4 FOR THE PSW MODEL IN THE PY AND HNC APPROXIMATIONS

Here the fourth virial coefficient predicted by the PY and HNC approximations from the various thermodynamic routes (v = virial, c = compressibility, e = energy) are given.

1. PY approximation

Using Eq. (6.1), along with the recursion relations (5.15)–(5.18), we have

$$
\begin{aligned}
B_4^{\mathrm{PY},v} &= \gamma_r^5 \left[3 - \gamma\Delta \left(9 - 7\Delta - 16\gamma\Delta + \Delta^2 + 6\gamma\Delta^2 + 6\gamma^2\Delta^2 - 2\gamma^3\Delta^2 \right) \right] \\
&\quad - \frac{\gamma_r^4}{2} \left[4 - \gamma\Delta \left(12 - 6\Delta - 18\gamma\Delta + \Delta^2 + 3\gamma\Delta^2 + 3\gamma^2\Delta^2 - 3\gamma^3\Delta^2 \right) \right],
\end{aligned}
\tag{C1}
$$

$$
\chi_4^{\mathrm{PY}} = -4 \left(2B_2^3 - 3B_2 B_3 + B_4^{\mathrm{PY},c} \right),
\tag{C2}
$$

$$
\begin{aligned}
B_4^{\mathrm{PY},c} &= \frac{\gamma_r^5}{3} \left[7 - \gamma\Delta \left(21 - 15\Delta - 36\gamma\Delta + 3\Delta^2 + 16\gamma\Delta^2 + 16\gamma^2\Delta^2 - 4\gamma^3\Delta^2 \right) \right] \\
&\quad - \frac{\gamma_r^4}{3} \left[4 - \gamma\Delta \left(12 - 6\Delta - 18\gamma\Delta + \Delta^2 + 3\gamma\Delta^2 + 3\gamma^2\Delta^2 - 3\gamma^3\Delta^2 \right) \right],
\end{aligned}
\tag{C3}
$$

$$
\begin{aligned}
u_4^{\mathrm{PY}} &= \frac{\gamma_r^3}{6} \left(1 + \gamma_r\gamma \right) \Delta \left[12 - 18\gamma_r - 6\Delta \left(1 - 2\gamma_r + 6\gamma - 10\gamma_r\gamma \right) + \Delta^2 \left(1 - 2\gamma_r + 6\gamma - 26\gamma_r\gamma + 9\gamma^2 - 36\gamma_r\gamma^2 \right. \right. \\
&\quad \left. \left. - 12\gamma^3 + 16\gamma_r\gamma^3 \right) \right] \epsilon_a - \frac{\gamma_r^3}{6} \left(1 - \gamma_r \right) \Delta \left[16 - 28\gamma_r - 6\gamma\Delta \left(6 - 11\gamma_r \right) + 6\gamma\Delta^2 \left(3 - 8\gamma_r + 6\gamma - 14\gamma_r\gamma \right) \right. \\
&\quad \left. - \gamma \left(1 + \gamma \right) \Delta^3 \left(3 - 10\gamma_r + 3\gamma - 28\gamma_r\gamma \right) \right] \epsilon_r.
\end{aligned}
\tag{C4}
$$

The fourth virial coefficient associated with the energy route, $B_4^{\mathrm{PY},e}$, is obtained from Eq. (C4) as

$$
B_4^{\mathrm{PY},e} = 3 \int_0^\beta d\beta' \, u_4^{\mathrm{PY}}(\beta').
\tag{C5}
$$

Its expression is quite long and so it is omitted here. In addition to its dependence on γ_r and γ, $B_4^{\mathrm{PY},e}$ depends on $\epsilon_a/(n_a\epsilon_a - n_r\epsilon_r)$ with $(n_a, n_r) = (1,1), (1,2), (1,3), (1,4), (2,1), (2,3), (3,1), (3,2), (4,1)$.

It is instructive to consider some special cases. First, the results for the PS model correspond to the limit $\epsilon_a \to 0$ ($\gamma \to 0$) or $\epsilon_a \to -\epsilon_r$ ($\gamma \to -1$):

$$
\lim_{\epsilon_a \to 0} B_4^{\mathrm{PY},v} = \lim_{\epsilon_a \to -\epsilon_r} \frac{B_4^{\mathrm{PY},v}}{(1+\Delta)^3} = \gamma_r^4 (3\gamma_r - 2),
\tag{C6}
$$

$$
\lim_{\epsilon_a \to 0} B_4^{\mathrm{PY},c} = \lim_{\epsilon_a \to -\epsilon_r} \frac{B_4^{\mathrm{PY},c}}{(1+\Delta)^3} = \gamma_r^4 \left(\frac{7\gamma_r}{3} - \frac{4}{3} \right),
\tag{C7}
$$

$$
\lim_{\epsilon_a \to 0} B_4^{\mathrm{PY},e} = \lim_{\epsilon_a \to -\epsilon_r} \frac{B_4^{PY,e}}{(1+\Delta)^3} = \gamma_r^4 \left(\frac{14\gamma_r}{5} - 2 \right).
\tag{C8}
$$

In the special case of the HPS model ($\epsilon_a < 0$ and $\epsilon_r \to 0$) one finds that $B_4^{\mathrm{PY},v}$ and $B_4^{\mathrm{PY},e}$ reduce to the exact result [see Eq. (5.28)] but $\lim_{\epsilon_r \to 0} B_4^{\mathrm{PY},c} = -\gamma_a^4\Delta^3$.

The conventional SW model corresponds to $\epsilon_r \to \infty$ ($\gamma_r \to 1$):

$$
\lim_{\epsilon_r \to \infty} B_4^{\mathrm{PY},v} = 1 - \gamma\Delta \left(3 - 4\Delta - 7\gamma\Delta + \frac{1}{2}\Delta^2 + \frac{9}{2}\gamma\Delta^2 + \frac{9}{2}\gamma^2\Delta^2 - \frac{1}{2}\gamma^3\Delta^2 \right),
\tag{C9}
$$

$$\lim_{\epsilon_r \to \infty} B_4^{\text{PY},c} = 1 - \gamma\Delta \left(3 - 3\Delta - 6\gamma\Delta + \frac{2}{3}\Delta^2 + \frac{13}{3}\gamma\Delta^2 + \frac{13}{3}\gamma^2\Delta^2 - \frac{1}{3}\gamma^3\Delta^2\right), \tag{C10}$$

$$\lim_{\epsilon_r \to \infty} B_4^{\text{PY},e} = \frac{4}{5} - \gamma\Delta \left(3 - 3\Delta - 6\gamma\Delta + \frac{1}{2}\Delta^2 + 5\gamma\Delta^2 + \frac{9}{2}\gamma^2\Delta^2 - \frac{1}{2}\gamma^3\Delta^2\right). \tag{C11}$$

If, furthermore, the SHS limit ($\gamma \to \infty$ and $\Delta \to 0$ with $\gamma\Delta = $ const) is taken in Eqs. (C9)–(C11), an artificial divergence of B_4 is obtained.

The results corresponding to HS are obtained by taking either the limit $\epsilon_r \to \infty$ ($\gamma_r \to 1$) in Eqs. (C6)–(C8) or the limit $\epsilon_a \to 0$ ($\gamma \to 0$) in Eqs. (C9)–(C11). In either case one sees that the virial and compressibility routes yield the exact result, while the energy route value is wrong by a factor 4/5. A third possibility consists of taking the limit $\epsilon_a \to -\infty$ ($\gamma \to -1$) in Eqs. (C9)–(C11). However, in this latter case the energy route yields an incorrect dependence on Δ:

$$\lim_{\epsilon_a \to -\infty} \lim_{\epsilon_r \to \infty} B_4^{\text{PY},e} = \frac{4}{5} + \frac{\Delta}{2} \left(6 + 6\Delta + \Delta^2\right). \tag{C12}$$

The fact that the right-hand side of Eq. (C12) is not proportional to $(1+\Delta)^3$ implies that if one starts from $B_4^{\text{PY},e}$ for the PSS model of shoulder height and width $-\epsilon_a$ and Δ, respectively, and then one takes the limit $\epsilon_a \to -\infty$ to get the HS model of diameter $1 + \Delta$, the result has an artificial dependence on Δ. This anomaly of the PY description was discussed in Ref. [34].

2. HNC approximation

Similarly to the preceding analysis, from Eq. (6.2) one gets

$$B_4^{\text{HNC},v} = \frac{3}{2} B_4^{\text{PY},c}, \tag{C13}$$

$$\chi_4^{\text{HNC}} = -4 \left(2B_2^3 - 3B_2 B_3 + B_4^{\text{HNC},c}\right), \tag{C14}$$

$$\begin{aligned}
B_4^{\text{HNC},c} &= \frac{5\gamma_r^5}{12} \left[7 - \gamma\Delta \left(21 - 15\Delta - 36\gamma\Delta + 3\Delta^2 + 16\gamma\Delta^2 + 16\gamma^2\Delta^2 - 4\gamma^3\Delta^2\right)\right] \\
&\quad - \frac{\gamma_r^4}{2} \left[4 - \gamma\Delta \left(12 - 6\Delta - 18\gamma\Delta + \Delta^2 + 3\gamma\Delta^2 + 3\gamma^2\Delta^2 - 3\gamma^3\Delta^2\right)\right],
\end{aligned} \tag{C15}$$

$$u_4^{\text{HNC}} = \frac{1}{3} \frac{\partial}{\partial\beta} B_4^{\text{HNC},v}, \tag{C16}$$

Equation (C16) implies that $B_4^{\text{HNC},e} = B_4^{\text{HNC},v}$. This confirms that, in general, the energy and virial routes are thermodynamically consistent in the HNC approximation [35]. It is also noteworthy that the fourth virial coefficient predicted by the HNC approximation in the virial and energy routes is exactly three halves the one predicted by the PY approximation in the compressibility energy route, Eq.(C13). This simple relation is not restricted to 1D models since it also occurs in the 3D PS model [17]. It would be extremely interesting to check whether relation (C13) is a general property valid for any interaction potential and for any dimensionality.

In the PS and SW limits Eq. (C15) becomes

$$\lim_{\epsilon_a \to 0} B_4^{\text{HNC},c} = \lim_{\epsilon_a \to -\epsilon_r} \frac{B_4^{\text{HNC},c}}{(1+\Delta)^3} = \gamma_r^4 \left(\frac{35\gamma_r}{12} - 2\right), \tag{C17}$$

$$\lim_{\epsilon_r \to \infty} B_4^{\text{HNC},c} = \frac{11}{12} - \gamma\Delta \left(\frac{11}{4} - \frac{13}{4}\Delta - 6\gamma\Delta + \frac{3}{4}\Delta^2 + \frac{31}{6}\gamma\Delta^2 + \frac{31}{6}\gamma^2\Delta^2 - \frac{1}{6}\gamma^3\Delta^2\right), \tag{C18}$$

respectively.

The three routes in the HNC theory yield the exact result (5.28) in the HPS limit. However, as in the case of the PY theory, an artificial divergence of B_4 is predicted in the SHS limit.

ACKNOWLEDGMENTS

[1] J.L. Barrat and J.P. Hansen *Basic Concepts for Simple and Complex Liquids* (Cambridge University Press, Cambridge, 2003).
[2] C.N. Likos, Phys. Rep. **348**, 267 (2001).
[3] C. Marquest and T.A. Witten, J. Phys. (France) **50**, 1267 (1989).
[4] Al. Malijevský and A. Santos, J. Chem. Phys. **124**, 074508 (2006).
[5] Z.W. Salsburg, R.W. Zwanzig, and J.G. Kirkwood, J. Chem. Phys. **21**, 1098 (1953).
[6] E. Tonks, Phys. Rev. **50**, 955 (1936).
[7] R.P. Feynman *Statistical Mechanics* (W.A. Benjamin, Reading, 1972).
[8] D.S. Corti and P.G. Debenedetti, Phys. Rev. E **57**, 4211 (1998).
[9] J.L. Lebowitz and D. Zomick, J. Chem. Phys. **54**, 3335 (1971).
[10] A. Santos, Phys. Rev. E **76**, 062201 (2007).
[11] N.A. Seaton and E.D. Glandt, J. Chem. Phys. **84**, 4595 (1986).
[12] S.B. Yuste and A. Santos, J. Stat. Phys. **72**, 703 (1993).
[13] M. Heying and D.S. Corti, Fluid Phase Equilibria **220**, 85 (2004).
[14] E.H. Lieb and D.C. Mattis, *Mathematical physics in one dimension* (Academic Press, New York and London, 1966); D. C. Mattis, *The Many-Body Problem: An Encyclopedia of Exactly Solved Models in One Dimension* (World Scientific, Singapore, 1993).
[15] R. Fantoni, Ph.D. thesis, University of Trieste, 2003 (unpublished).
[16] It may be useful to stress that in quantum statistical mechanics the condition of impenetrability in a one-dimensional fluid with periodic boundary conditions is responsible for the impossibility to treat the particles just as fermions or bosons but one necessarily has to introduce the anyonic fractional statistics. In classical statistical mechanics the change in the topology of phase space does not have such a dramatic consequence.
[17] A. Santos and Al. Malijevský, Phys. Rev. E **75**, 021201 (2007).
[18] M.E. Fisher and D. Ruelle, J. Math. Phys. **7**, 260 (1966).
[19] D. Ruelle, *Statistical Mechanics: Rigorous Results* (Benjamin, London, 1969).
[20] B. Widom and J.S. Rowlinson, J. Chem. Phys. **52**, 1670 (1970).
[21] S. Torquato, J. Chem. Phys.**81**, 5079 (1984)
[22] P.A. Rikvold and G. Stell, J. Collid Interface Sci., **108**, 158 (1985); P.A. Rikvold and G. Stell, J. Chem. Phys. **82**, 1014 (1985).
[23] A.A. Louis, P.G. Bolhuis, and J.P. Hansen, **62**, 7961 (2000).
[24] D.M. Heyes, M.J. Cass, and G. Rickayzen, J. Chem. Phys. **126**, 084510 (2007).
[25] R.J. Baxter, J. Chem. Phys. **49**, 2770 (1968).
[26] R. Fantoni, D. Gazzillo, A. Giacometti, M. Miller, and G. Pastore, J. Chem. Phys. **127**, 234507 (2007).
[27] G. Stell, J. Stat. Phys. **63**, 1203 (1991).
[28] R. Kikuchi, J. Chem. Phys. **23**, 2327 (1955).
[29] Z. Elkoshi, H. Reiss, and A.D. Hammerich, J. Stat. Phys. **41**, 685 (1985).
[30] J-P. Hansen and I.R. McDonald, *Theory of Simple Liquids*, 3rd. ed. (Academic Press, London, 2006).
[31] Note that the cancellation of these three singularities do not occur in the HNC approximation, where $y_{2D}^{(\mathrm{SHS})}(r)$ is neglected. In the PY approximation both $y_{2C}^{(\mathrm{SHS})}(r)$ and $y_{2D}^{(\mathrm{SHS})}(r)$ are neglected, so that the singularities (i) and (ii) persist.
[32] L. Acedo and A. Santos, Phys. Lett. A **323**, 427 (2004).
[33] J.A. Cuesta and A. Sánchez, J. Stat. Phys. **115**, 869 (2004).
[34] A. Santos, Mol. Phys. **104**, 3411 (2006).
[35] T. Morita, Prog. Theor. Phys. **23**, 829 (1960); see also p. 636 of J. A. Barker and D. Henderson, Rev. Mod. Phys. **48**, 587 (1976).